FIRST RESULTS FROM JADE

JADE Collaboration[1]

Presented by S. Orito, LICEPP, The University of Tokyo, Japan

Abstract

First results from the JADE experiment at the highest PETRA energies ($\sqrt{s}$ = 22 to 31.6 GeV) are reported. QED is tested using the reactions $e^+e^- \to e^+e^-$ and $\gamma\gamma$ and found valid down to distances of 2×10^{-16} cm. Fits to the differential cross section for $e^+e^- \to e^+e^-$ provide constraints on models of the weak-electromagnetic interaction. For the reaction $e^+e^- \to$ multihadrons an average R value of 4.1 ±0.3 is obtained in the above energy range, compatible with production of quarks with only the known flavours (u, d, s, c, b). Topological distributions of the hadrons are studied in search of deviations from a narrow two-jet structure. No evidence is observed for spherical events, which would be expected from the production of heavy particles bearing a new flavour. However, broadening of jets and an excess of planar events are observed at a rate which cannot be explained by statistical fluctuations in the two-jet mechanism. The planar events exhibit distinct three-jet structures in many cases. If gluon bremsstrahlung $e^+e^- \to q\bar{q}g$ is included, detailed agreements are obtained between the predictions and data. This strongly suggests gluon bremsstrahlung as the origin of jet broadening and planar three-jet events. Free fractionally charged or heavy stable particles are searched for in the multihadron sample and upper limits for production cross sections are obtained. The azimuthal angular distributions of both inclusive hadrons and jet axes show a $\cos 2\phi$-like modulation, compatible with a large vertical beam polarization.

Introduction

The JADE experiment is being carried out at the e^+e^- colliding beam facility PETRA by a collaboration of physicists[1] from DESY, the Universities of Hamburg, Heidelberg, Lancaster and Manchester, the Rutherford Laboratory and the University of Tokyo. The experiment was proposed[2] in 1976 as a compact solenoidal detector with 4π coverage for charged particle and photon detection as well as for lepton (e and μ) identification. The construction phase ended in spring of this year. Data taking started at the end of June with the whole of the proposed detector in position. All data taken before this symposium have been analyzed and will be reported on here. All results should be considered as preliminary.

During the data taking PETRA operated at total C. M. energies ($\sqrt{s}$) from 22 to 31.6 GeV. Instantaneous luminosities up to 2×10^{30} cm^{-2} sec^{-1} were obtained with two bunches of e^+ and two bunaches of e^- and typical currents of 3 mA per bunch.

1. Detector

Fig. 1 shows a sectional view of the JADE detector in a vertical plane containing the beam axis. A normally conducting aluminium coil of 7 cm thickness and 2 m diameter produces a uniform solenoidal field of maximum strength 0.5 Tesla over a length of 3.5 m. Inside the coil the passage of charged particles is recorded by a Beam Pipe Hodoscope (24 counters) and a Time of Flight Hodoscope (42 counters).

The trajectories of the charged particles are measured by a cylindrical drift chamber, called the "Jet chamber" [3]. 48 points are measured along each track in the polar angular range $|\cos\theta| < 0.83$ and at least 8 points on a track are obtained over a solid angle of 97 % of the full sphere. At each point, three coordinates, r, ϕ and z are given by the wire position, the drift time and the charge division measurements. dE/dx information, which is used for particle identification, is also obtained. The gas mixture of Argon-Methane-Isobutane is used under 4 times atmospheric pressure.

The magnet coil is surrounded by 30 rings of lead glass shower counters covering the angular range $|\cos\theta| < 0.82$. Each ring contains 84 glass wedges (Schott SF5) with inner surfaces of 85 x 102 mm^2 and depths of 300 mm (12.5 X_0). These 2520 barrel shower counters, together with the 192 shower counters mounted inside the magnet on the two end caps of the yoke, cover 90 % of the full solid angle and serve to detect and measure the energies of photons and electrons. The fine granularity of the shower counters allows a measurement of the photon emission angles to ±2 degrees using the known interaction point. It should be noted that the inner part of the JADE detector (hodoscopes, the drift chamber and the shower counters) have complete rotational symmetry in the azimuthal angle.

The flux return yoke, including the end caps, forms a rectangular box surrounding the cylindrical part of the detector. It is utilized as one of the layers of the muon filter and is followed by three further layers consisting of iron loaded concrete. The total thickness of absorber amounts to at least 780 g/cm^2 (6 absorption lengths). It is interspersed with 5 layers of drift chambers which measure the trajectories of penetrating particles with a coverage of 92 % of the full solid angle.

Two small angle detectors, each consisting of an array of scintillation counters, drift chambers and lead glass modules, record electrons and positrons close to the beam direction ($35 < \theta < 75$ mrad). They provide an on-line measurement of the luminosity and tag the two-photon processes ($e^+e^- \to e^+e^-$ + hadrons).

There are two types of trigger relevant to the results presented here. The "charged-particle trigger" requires

1) at least two time of flight counter hits,
2) total shower energy (sum of the barrel and end caps) more than 1 GeV, and
3) at least one track recognized by the track logic based on the hit pattern of the drift chamber wires.

The "shower-energy trigger" on the other hand is based exclusively on the shower energy and requires a total of more than 4 GeV in coincidence with the crossing of the beams. These two triggers are largely redundant since more than 95 % of the finally accepted multihadron events and 100 % of the Bhabha events satisfy both trigger conditions.

The absolute luminosity was obtained from Bhabha scattering in the end cap lead glass counters ($0.91 < \cos\theta < 0.96$). The effect of a possible QED breakdown is less than 1 % in this angular range.

Fig. 2 shows a typical multihadron event recorded in the JADE detector. Trajectories of charged and neutral particles are represented by full and dotted lines, respectively. The advantage of having a dense track

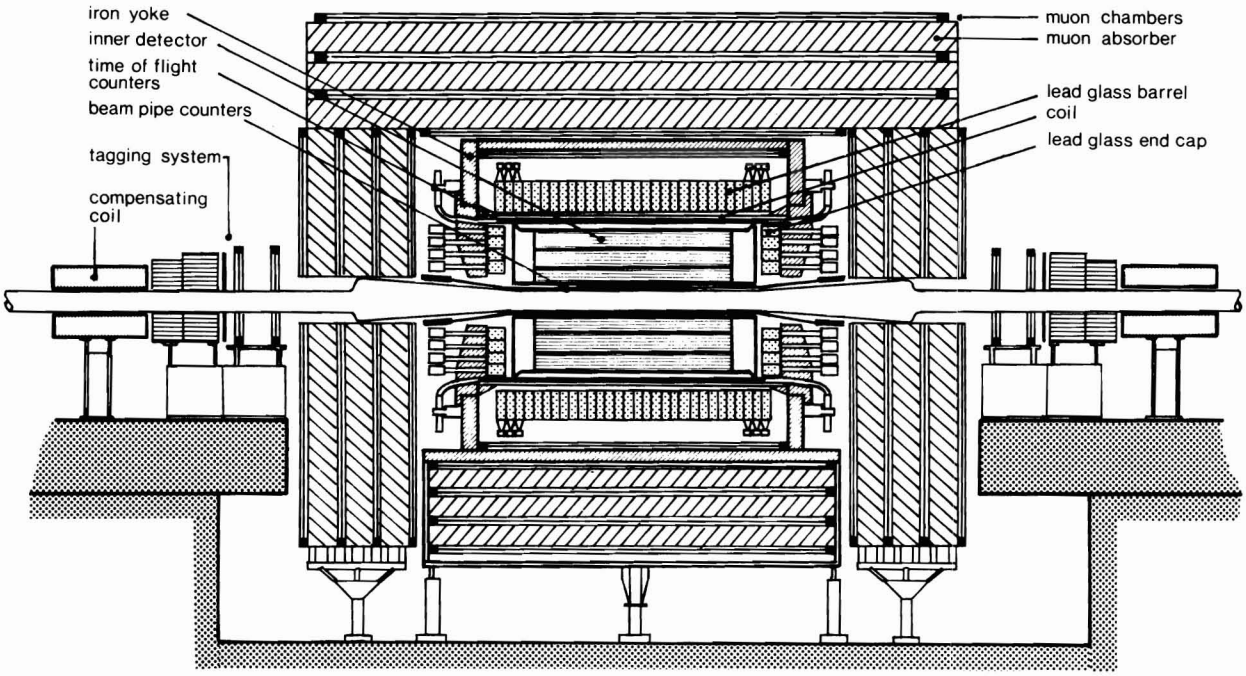

Fig. 1: A sectional view of the JADE detector in a vertical plane containing the beam axis.

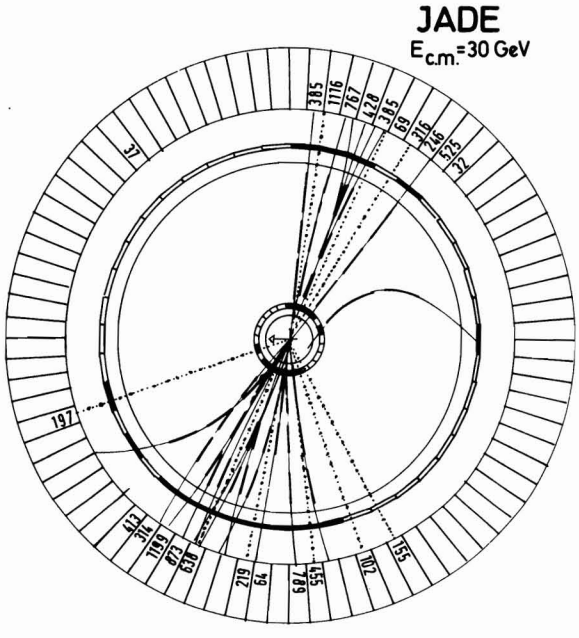

Fig. 2-a: A typical multihadron event (view along the beam) recorded in the central part of the JADE detector.
Trajectories of charged and neutral particles are represented by full and dotted lines respectively. The shower counters are also shown here, each wedge representing a row of 30 lead glass counters. The energy deposited in each of these rows appears in units of MeV.

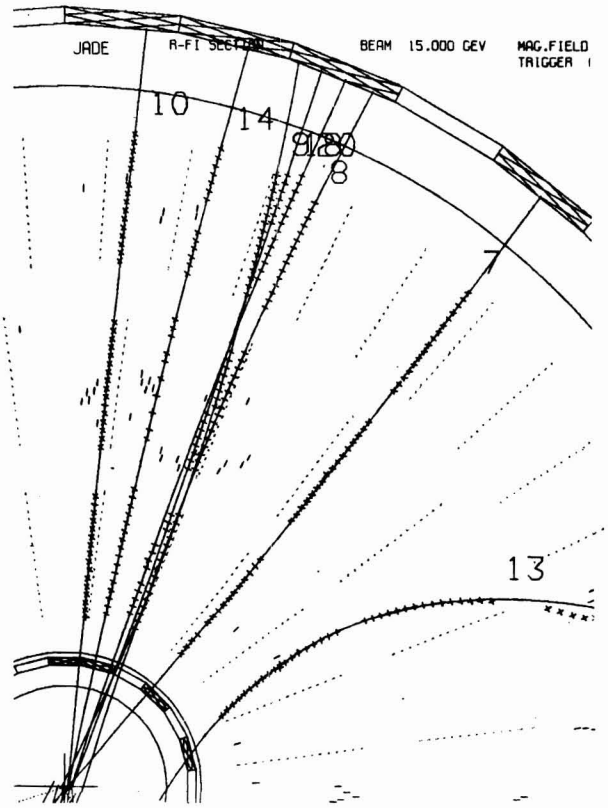

Fig. 2-b: A close up view of the same event as shown in Fig. 2a.
The faint dots indicate the positions of the sense wires. Each track is seen to be defined by up to 48 independent coordinate measurements.

sampling and finely segmented shower counters in analyzing a complicated event is apparent from this figure.

2. QED Test

The reactions $e^+e^- \to e^+e^-$ and $\gamma\gamma$ were analyzed in order to test quantum electrodynamics at the available q^2's of up to 900 GeV^2. The Bhabha and $\gamma\gamma$ events were identified by requiring two collinear showers each with at least 1/3 of the beam energy. The Bhabha events were further separated from the $\gamma\gamma$ events by requiring that each shower be associated with a track in the jet chamber. Samples of the Bhabha and $\gamma\gamma$ events were visually scanned to assure a negligible background (<1 %) over all angular region.

The acollinearity distribution for the Bhabha events is shown in fig. 3. Excellent agreement with the QED prediction[4,5] is obtained for acollinearities from 0^o to 40^o, suggesting a very low level of background. For events in the barrel a polar angle acceptance cut of $|\cos\theta| < 0.77$, well inside the actual coverage of the shower counters, and a maximum acollinearity cut of 10^o were applied. These minimize geometrical edge effects. Remaining small (<5 %) edge losses were corrected by a Monte Carlo simulation[5].

The cross sections presented here are integrated over all azimuthal angles. Since the relevant parts of the detector have full azimuthal symmetry, this ensures that the resulting cross sections will not be affected by any transverse beam polarization.

Fig. 4 shows the results. The weighted cross sections $s \cdot d\sigma/d\Omega$ for Bhabha and $\gamma\gamma$ reactions at various $\sqrt{s}$'s are plotted versus $\cos\theta$. The QED prediction[6] (solid curves in fig. 4) includes radiative corrections up to order α^3 as well as the contribution from hadronic vacuum polarization. Excellent agreements between the data and the QED predictions are observed for both reactions at all energies.

In order to express the agreement quantitatively a possible breakdown of QED is parametrized[7] for $e^+e^- \to \gamma\gamma$ by:

$$\frac{d\sigma}{d\Omega} = \left(1 \pm \frac{s^2}{2\,\Lambda_\pm^4} \sin^2\theta\right) \left(\frac{d\sigma}{d\Omega}\right)_{QED}$$

A χ^2 fit to all of the $\gamma\gamma$ data using the above formula provides limits:

$$\Lambda_+ > 43 \text{ GeV} \quad \text{and} \quad \Lambda_- > 31 \text{ GeV}$$

(95 % confidence level)
The cut-off parameter Λ_+ can be regarded[7] as the ratio of the mass to the coupling constant of a possible heavy electron which might mediate the reaction.

For Bhabha scattering a possible QED breakdown is parametrized according to a hypothetical modification[8] of the photon propagator. The standard QED propagator is multiplied by a form factor:

$$F(q^2) = 1 \pm q^2/(q^2 - \Lambda_\pm^2)$$

A χ^2 fit for all data points provides limits:

$$\Lambda_+ > 89 \text{ GeV} \quad \text{and} \quad \Lambda_- > 74 \text{ GeV}$$

(95 % confidence level)
The validity of QED and the point-like nature of $e^\pm$ are thus tested to distances as small as 2×10^{-16} cm.

The Bhabha data were also fitted to the theoretical cross section incorporating the standard Weinberg-Salam model[9] with $\sin^2\theta_W$ as the free parameter. A limit

$$\sin^2\theta_W < 0.66 \quad (95\ \%\ \text{confidence level})$$

is obtained. It should be noted that this is the first test of the model at such high q^2.

The Bhabha scattering data can also be used to test other models of weak electromagnetic interactions. Especially interesting are the models which reproduce the predictions of the standard Weinberg-Salam model at zero q^2 but possess a rich neutral boson structure, usually with one neutral boson below the Weinberg-Salam neutral boson. Low q^2 experiments cannot distinguish these from the standard model. Our data at high energy, however, would be sensitive to the existence of a neutral boson with a mass not too far above the available energy. A two-pole model by de Groot et. al[10] was taken as an example and a fit was made to the Bhaba data. The two independent parameters of the model were chosen to be the width Γ_1 and the mass M_1 of the lighter neutral boson. The result is shown in fig. 5. Our data exclude at a 95 % confidence level the indicated region in the Γ_1 - M_1 plot for this model.

3. Selection of the $e^+e^- \to$ Multihadron Events

Multihadron candidates were selected by off-line analysis using the following criteria:

1) At least 2 tracks must pass through a cylindrical fiducial volume considerably larger than the size of the interaction region folded with the resolution of the detector. In addition an acoplanarity angle of more than 10^o is required for events with only two tracks. These cuts suppress cosmic ray and QED backgrounds.

2) The barrel shower energy must be greater than 2 GeV at $\sqrt{s}$ = 22 GeV and greater than 3 GeV at higher energies, or both end cap shower energies must be greater than 0.4 GeV.

Surviving events were scanned by at least two physicists independently. Any backgrounds from cosmic rays or showering e^+e^- or $e^+e^-\gamma$ events were removed and any deficiencies in the pattern recognition were rectified. After these visual checks, a further selection of events with at least 4 tracks was made in order to reduce the background from $e^+e^- \to \tau^+\tau^-$. The $\tau^+\tau^-$ background was further minimized by rejecting 4 track events if three of the charged tracks were in nearly the opposite direction to the fourth.

The total visible energy and the longitudinal momentum balance were calculated for these events in the following way:

$$\text{Total visible energy} = E_{vis} = \sum_i E_i$$

$$\text{Longitudinal momentum balance} = B_L = \sum_i p_i \cos\theta_i / E_{vis}$$

where the sums are taken over charged and neutral particles. Particle masses were neglected in calculating energies. Fig. 6a shows a correlation plot for momentum balance versus total visible energy for data at $\sqrt{s}$ = 27.7 GeV. A cut of $|B_L| < 0.4$ was applied to reduce the backgrounds from beam-gas and two-photon processes. Fig. 6b shows the visible energy distribution after this momentum balance cut together with the expected background from the two-photon processes[11]. A further cut of E_{vis} > beam energy eliminated the remaining beam-gas background and reduced the level of two-photon events to about 1 %. This amount was verified by Monte-Carlo simulation and subtracted. The residual background from $\tau^+\tau^-$ was also estimated by a Monte-Carlo simulation to be about 2 % and subtracted.

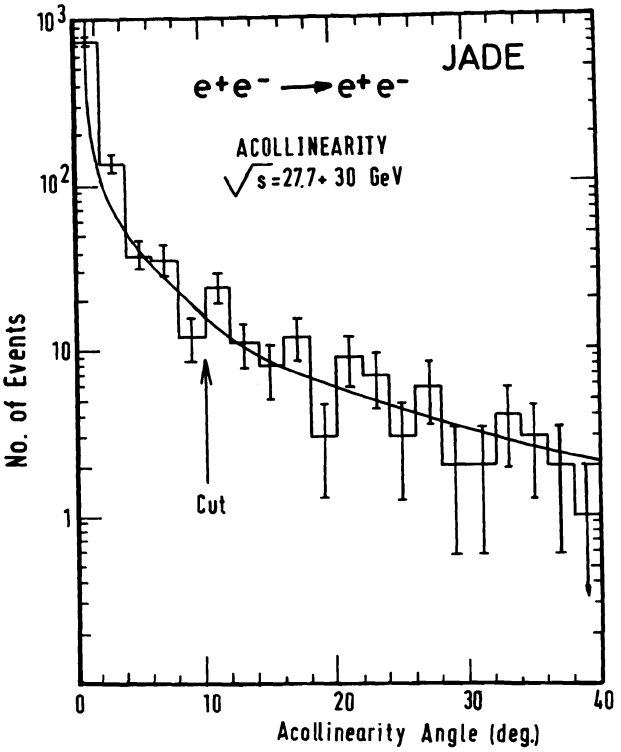

Fig. 3: The acollinearity angle distribution of the Bhabha events.

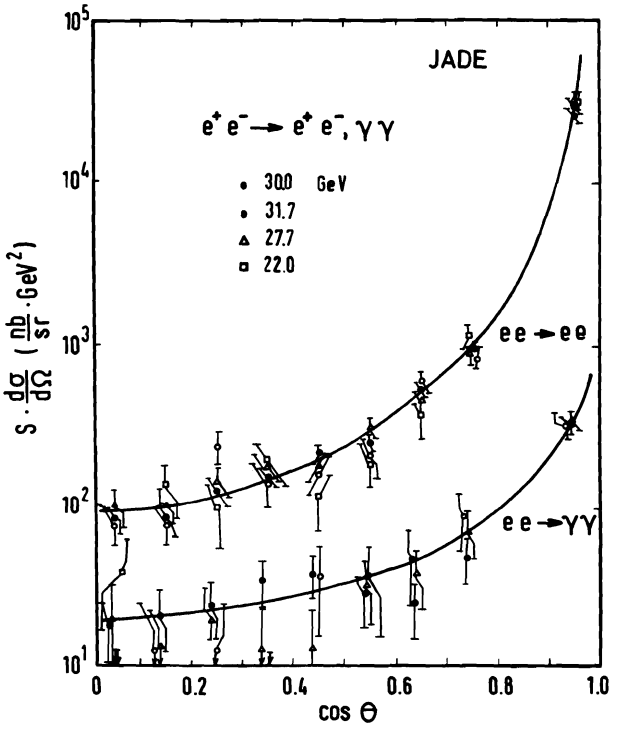

Fig. 4: QED result: $S \cdot \frac{d\sigma}{d\Omega}$ as function of $\cos\theta$ for $e^+e^- \to e^+e^-$ and $\gamma\gamma$ events at four different $\sqrt{s}$.
The curves show QED predictions.

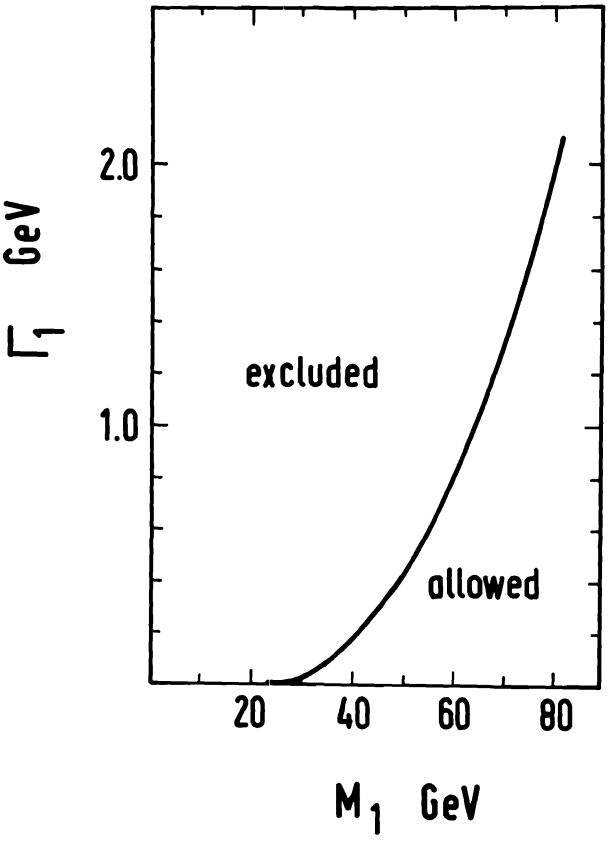

Fig. 5: Allowed and excluded regions for the two-pole model of de Groot et al. The width of the lighter neutral weak boson is plotted versus its mass.

4. R and Multiplicity

The efficiencies of the trigger and the off-line selections were determined by Monte-Carlo simulation using a jet model[12,13] including u, d, s, c and b flavour production ($q\bar{q}$ model explained below). The incident e^+ and e^- beams were allowed to radiate photons according to the formula of Bonneau and Martin[4] to a maximum energy of $k_{max} = 0.95\ E_{beam}$. This simulation results in a radiative correction factor of $1+\delta = 1.21$ to the total cross section and a detection efficiency of $\varepsilon = 0.82$ as compared with efficiency of 0.88 without the radiative loss. The product $\varepsilon\ (1 + \delta)$, which determines the overall correction, is insensitive to the precise value of k_{max}.

The result is summarized in table 1, where the R values (total hadronic cross section in unit of point-like $\mu\mu$ cross section) are given at various $\sqrt{s}$'s.

Table 1 R values and the averaged charged multiplicites

$\sqrt{s}$ GeV	Luminosity nb^{-1}	No. of events	R	$\langle n_{ch} \rangle$
22	39	21	2.9 ±0.7	10.1 ±0.7
27.7	192	89	4.0 ±0.5	11.6 ±0.5
30	438	198	4.6 ±0.4	11.7 ±0.5
31.6	132	49	4.2 ±0.6	10.9 ±0.6

Average (22 - 31.6 GeV) = 4.14 ±0.26

The errors quoted are statistical only. To estimate the systematic error in the efficiency determination, two further jet models were used, one[14] with different decay matrix elements for the heavy mesons and the other including gluon effect (the $q\bar{q}g$ model[15] explained below). The efficiencies from the three different jet models agreed to within 5 %.

The integrated luminosities determined from the end cap Bhabha scattering agree with the result obtained from the small angle luminosity monitor within 3 % and with the result from large angle Bhabha scattering to within a similar amount.

It should be pointed out that a longitudinal polarization h_μ of the beams, if present, would change[16] the observed cross section for the production of multihadron events by a factor of $(1 - h_\mu^2)$, whereas the measured luminosity would remain practically unaffected. An upper limit on this effect can be obtained from the reactions $e^+e^- \to \gamma\gamma$ and $\to e^+e^-$, which are also affected by longitudinal polarization[16]. The differential cross sections measured by JADE agree with QED at all energies within the statistical error and provide an upper limit (95 % C.L.) of $h_\mu^2 < 0.15$ at $\sqrt{s} = 27.7$ and 30 GeV and $h_\mu^2 \leq 0.3$ at $\sqrt{s} = 22$ and 31.6 GeV.

The R values are plotted in fig. 7 together with published data[17] and are compared with the quark-parton model predictions with QCD correction[18]. Our R values are consistent with the production of quarks with only the known flavours (u, d, s, c and b). No significant anomaly is observed[19] in the $\sqrt{s}$ dependence of R.

Charge multiplicities were determined for the multihadron events. Jet-like events with the jet axis at a small angle to the incident beam ($\theta < 40^o$) were excluded in order to avoid possible loss of particles in the beam direction. Any e^+e^- pairs from converted photons were also not included. The resulting average charge multiplicities are given in table 1 and are plotted in fig. 8 together with previously published data[20]. The errors quoted are statistical only whereas systematic errors are estimated to be about 1.5. The selection of events with at least 4 tracks is expected to result in a negligible bias according to the jet model[12,13].

As seen in fig. 8 a simple ln S law cannot fit the data. A $(\ln S)^2$ term or $s^{1/4}$ dependence[21] is needed to fit the observed rapid increase of the charged multiplicity with increasing $\sqrt{s}$.

5. Search for New Flavour Production

The decays of heavy particles bearing new flavours are expected to result in relatively spherical hadron distributions in contrast to the narrow jet-like distributions from known, low mass flavours. The topological distribution of multihadron events was studied in search of open production of a new flavour.

To this purpose the normalized sphericity tensor[22] was constructed and diagonalized for each event:

$$T_{\alpha\beta} = \sum_i P_{i\alpha} P_{i\beta} / \sum_i P_i^2$$

where $P_{i\alpha}$ is the α-component (α = x, y, z) of the momentum of the i-th particle. The sum was taken over charged and neutral particles. The resulting eigenvalues Q_1, Q_2, Q_3 ($Q_1 < Q_2 < Q_3$) are proportional to the lengths of the orthogonal axes of the momentum elipsoid, and satisfy the constraint $Q_1 + Q_2 + Q_3 = 1$. Each event is then represented by a point in a triangle plot as shown in fig. 9a.

This figure contains all events from the various C.M. energies. No significant accumulation of "spherical" events is observed in the upper part of the triangle if this figure is compared with the result of a Monte Carlo simulation for Top[23] particle production (fig. 9b). In this simulation[13] Top mesons were produced in pairs with cross section $\sigma_{t\bar{t}} = 4/3\ \sigma_{\mu\mu}$, together with u, d, s, c and b flavours, and allowed to decay in the chain $t \to b \to c$.

For a quantitative comparison the events were counted inside the cuts sphericity = $3/2(Q_1 + Q_2) > 0.55$ and $Q_1 > 0.075$, which are designed to select spherical events while excluding most of the two-jet events.

Table 2 summarizes the numbers of events expected inside this cut for Top meson masses of 8, 11 and 14 GeV at various $\sqrt{s}$, and compares them to the observed numbers of events.

Table 2 The number of spherical (sphericity > 0.55 and $Q_1 > 0.075$) events expected from production of Top mesons, compared with observed number of events

	m_t (GeV)	$\sqrt{s}$ (GeV)			
		22	27.7	30	31.6
number of events expected	8	4	3	2	0
	11	-	15	22	4
	14	-	-	25	5
number of events observed	-	0	1	1	1

No indication for spherical events is obtained at any $\sqrt{s}$. The data are not consistent with production of Top mesons with a mass between 11 and 14 GeV at the rate assumed above.

Phase space decay of the Top mesons results in a similar number of expected events. This indicates that the above conclusion is not affected by the detailed decay mechanism of the Top meson. However, it should be

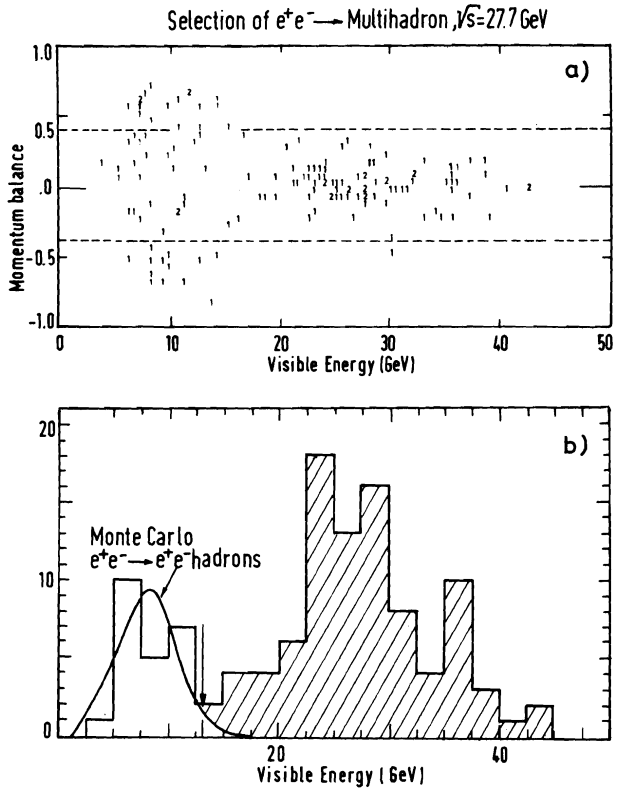

Fig. 6: a) Longitudinal momentum balance versus visible energy for the e^+e^- → multihadron candidates at $\sqrt{s}$ = 27.7 GeV. The dotted lines indicate the cut |momentum balance| < 0.4.

b) The visible energy distribution after the momentum balance cut. The cut $E_{vis} > E_{beam}$ is indicated by an arrow. The curve represents the expected background from the two-photon processes using a $\gamma\gamma$ total hadronic cross section of 260 nb.

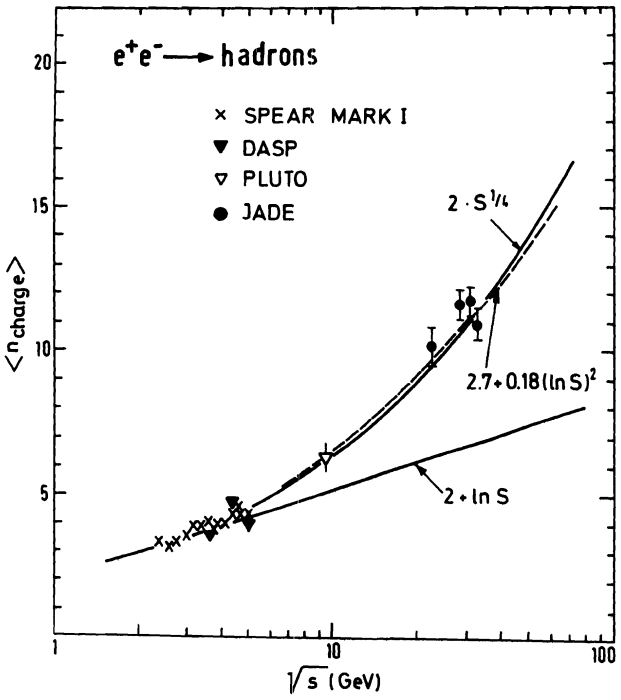

Fig. 8: Mean charged multiplicity as function of $\sqrt{s}$.

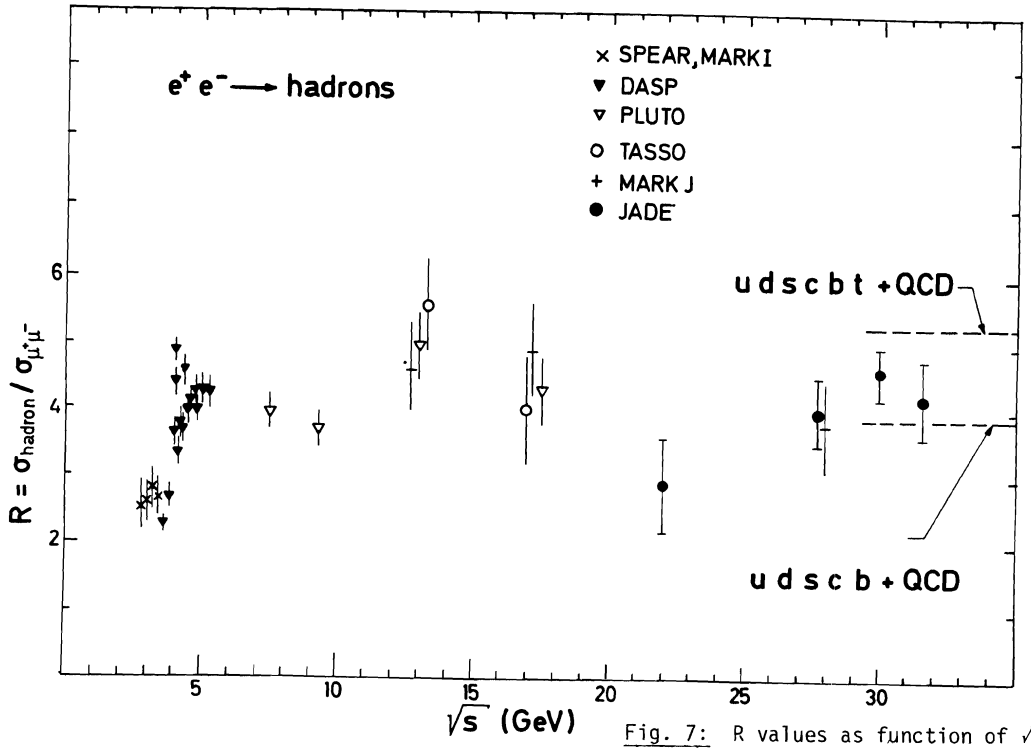

Fig. 7: R values as function of $\sqrt{s}$.

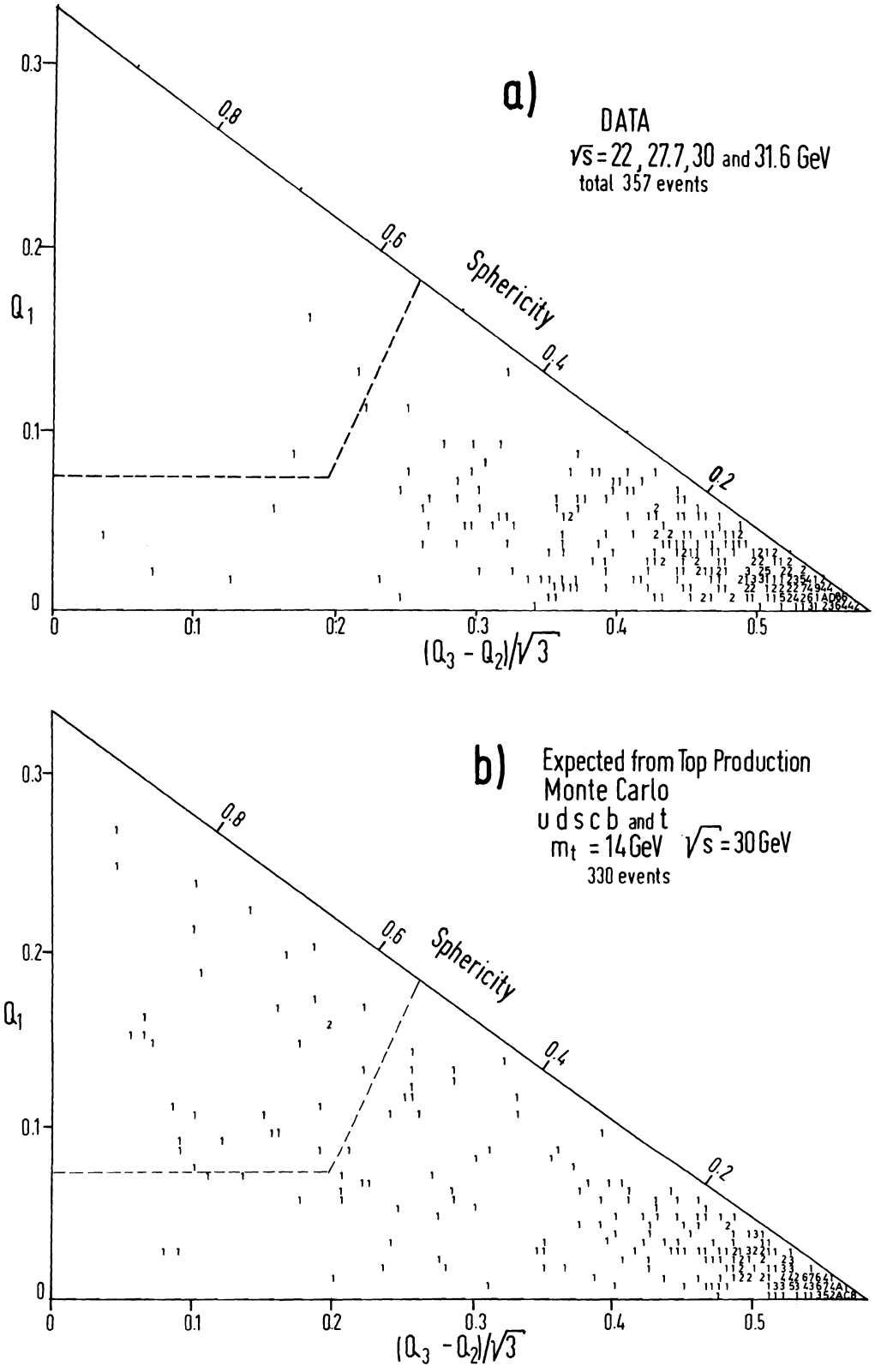

Fig. 9: "Event shape" Q-plots as defined in the text.

a) Combined data from all energies. The cut for spherical events ($s>0.55$ and $Q_1>0.075$) is indicated by dotted lines.

b) Monte Carlo prediction with open top production.

noted that this analysis assumes multihadron decays of the new heavy particle.

6. Evidence for Planar Three-Jet Events

The perturbative QCD theory of strong interactions predicts[24] a specific type of deviation from two-jet structure due to the gluon bremsstrahlung process $e^+e^- \to q\bar{q}g$. Soft bremsstrahlung of gluons at small angles to the quark direction will cause a broadening of one of the two jets, whereas hard bremsstrahlung at large angles will produce a well defined event plane containing the quark, antiquark and gluon, which then fragment into three distinct jets. Therefore, in addition to the predominant two-jet topology, the data should contain a subset of events with a planar configuration, of which a fraction should exhibit a distinct three-jet like structure.

To study these QCD effects the data were analysed as follows. First, a comparison was made between the data and a two-jet model. This established the jet broadening and the excess of planar events. Second, the data were compared with a jet model which included gluon bremsstrahlung $q\bar{q}g$ in addition to $q\bar{q}$.

The $q\bar{q}$ model[12,13] included production of u, d and s quarks which decayed with fragmentation function $f(z) = 1 - a + 3a(1 - z^2)$, where $a = 0.77$, and production of c and b quarks with fragmentation function[12] $f(z) = \text{const}$. The transverse momentum (q_T) distribution of the secondary quarks in the hadron-jet cascades was described by $d\sigma/d^2q_T \sim \exp(-q_T^2/2\sigma_q^2)$, where two values of σ_q were used, a standard value of 250 MeV/c, with which the $q\bar{q}$ model adequately describes low energy data[25] and an arbitratily large value of 350 MeV/c, which was used for comparison purposes.

In the $q\bar{q}g$ model[15] the u, d, s, c and b quarks were produced in the same way, but the u, d, s and c quarks were then allowed to radiate vector gluons with a probability given by QCD. The quark fragmentation functions were as defined above and the gluon fragmentation function was taken to be $f(z) = (1 - z)^2$. A σ_q value of 250 MeV/c was used both for the quark and the gluon fragmentation. The events are generated according to these models by a Monte Carlo program in which hard photon radiation[4] by the initial beams is taken into account. Then the events are followed through the detector and analyzed in exactly the same way as the real data.

The jet characteristics were studied by determining the quantity thrust[26] $T = \max(\sum_i |p_{\parallel i}|)/(\sum_i |p_i|)$ for each event. The longitudinal axis along which the value of T is maximised provides a good estimate of the jet axis, and the magnitude of T indicates how jet-like the event is. The limiting values of T are $T_{min} = 0.5$ (spherical) and $T_{max} = 1.0$ (extreme jet). Fig. 10 shows our measured thrust distributions compared with the predictions of the simple $q\bar{q}$ model. A main feature of the data is a sharp peak at high thrust as expected from the two-jet model. The data show, however, an excess of low thrust events compared with the $q\bar{q}$ model expectation. The production of a new flavour (e.g. Top) has already been excluded as a possible origin of this broadening on the basis of the total cross section measurement and the absence of spherical events.

Next we study transverse momentum distributions of charged particles to see whether particle momenta tend to lie in a plane. We define the mean p_T^2 components normal to and in the event plane ($\vec{n}_3$ - $\vec{n}_2$ plane), respectively, by

$$\langle p_T^2 \rangle_{out} = \frac{1}{N} \sum_{j=1}^{N} (\vec{p}_j \cdot \vec{n}_1)^2$$

and

$$\langle p_T^2 \rangle_{in} = \frac{1}{N} \sum_{j=1}^{N} (\vec{p}_j \cdot \vec{n}_2)^2.$$

Fig. 11 shows the $\langle p_T^2 \rangle_{out}$ and $\langle p_T^2 \rangle_{in}$ distributions for the high energy data[27] compared with $q\bar{q}$ model predictions. An excess of events with high $\langle p_T^2 \rangle_{in}$ is observed in the form of a long tail and is not compatible with the model prediction. This indicates that the data contain "planar" events. The rate of such planar events cannot be explained as a statistical fluctuation of the simple two-jet process.

A more thorough analysis can be made by studying the detailed event shapes. Fig. 12a shows the triangle Q-plot for the high energy data. If compared with the $q\bar{q}$ model prediction shown in fig. 12b, a substantial deviation from the two-jet model is apparent: the data contain an excess of planar events with small Q_1 and large $Q_3 - Q_2$. Quantitatively, there are 23 events in the region of the $1/\sqrt{3}\,(Q_3 - Q_2) < 0.35$ and $Q_1 < 0.07$ compared to a prediction of 6 from the $q\bar{q}$ model (see table 3).

Fig. 13 shows a projection of the Q plot onto the $Q_2 - Q_1$ (planarity) axis. The data show a considerable excess of events with high values of $Q_2 - Q_1$ (planar events) compared with the prediction of the $q\bar{q}$ model. For the region $Q_2 - Q_1 > 0.07$, we observe 78 events, whereas 24 events would be expected on the basis of the simple $q\bar{q}$ model with $\sigma_q = 250$ MeV/c (see table 4). It can be seen from the curves in fig. 13 that an arbitrary increase in σ_q from 250 to 350 MeV/c still cannot account for the excess of events.

Therefore, we see, at this high energy, jet broadening and an excess of planar events incompatible with the simple $q\bar{q}$ model. The existence of planar events strongly suggest a three-body primary process such as $e^+e^- \to q\bar{q}g$. Since the total energy available (30 GeV) is sufficient to collimate the 3 resulting jets to the extent that the primary plane is still well defined, a significant fraction of the events should demonstrate a three-jet structure. A number of such events is actually found among the planar events. Fig. 14 shows three such events projected onto the $\vec{n}_3$ - $\vec{n}_2$ and $\vec{n}_2$ - $\vec{n}_1$ planes. The momentum vectors of charged and neutral particles are represented by solid and dotted lines. The total energy flow is shown by the histogram plotted on a circle around the event. Three distinct clusters of energy flow can be seen in all of the events, indicating three-jet structure.

In order to study the origin of the planar and three-jet events we obtained various expected distributions from the $q\bar{q}g$ model and compared them with the measured thrust distribution (fig. 10), the triangle Q plot (fig. 12 and table 3) and the planarity (fig. 13 and table 4) distribution.

Table 3 Observed and expected numbers of events inside the cut

$(Q_3 - Q_2)/\sqrt{3} < 0.35$ and $Q_1 < 0.07$

observed	expected	
	$q\bar{q}$ model $\sigma_q = 250$ MeV/c	$q\bar{q}g$ model
23 events	6 events	22 events

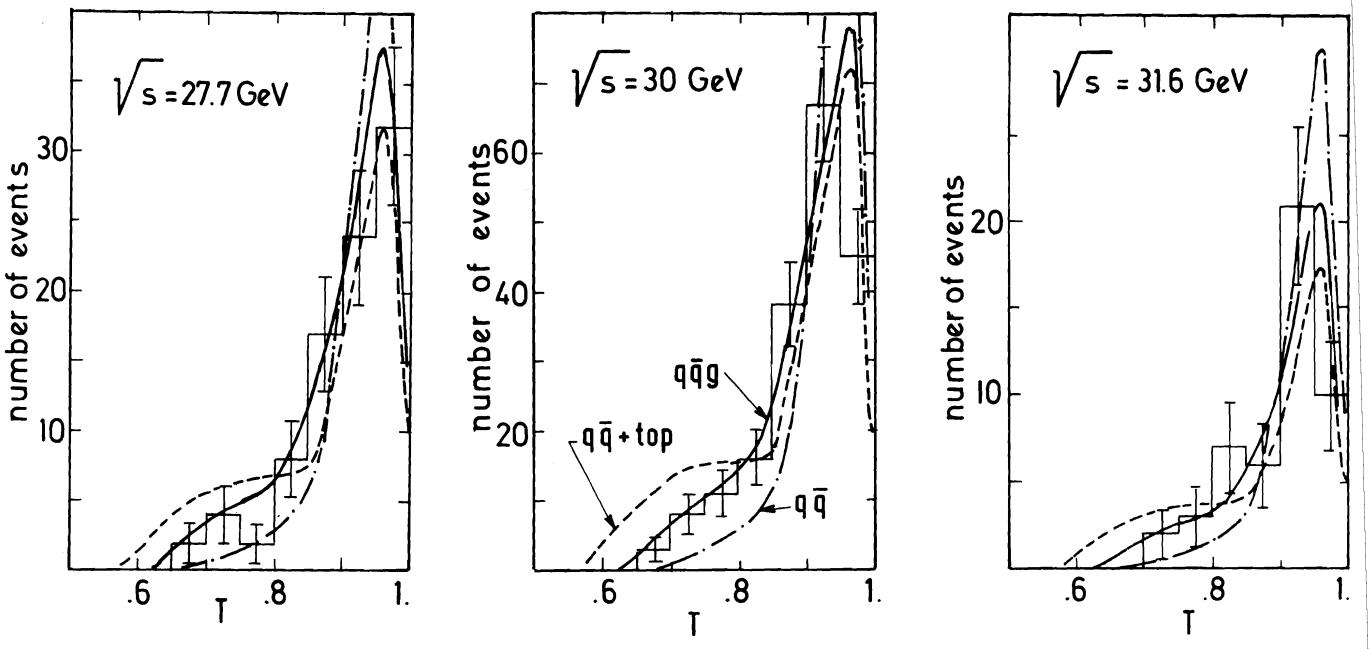

Fig. 10: The thrust distributions at various $\sqrt{s}$.

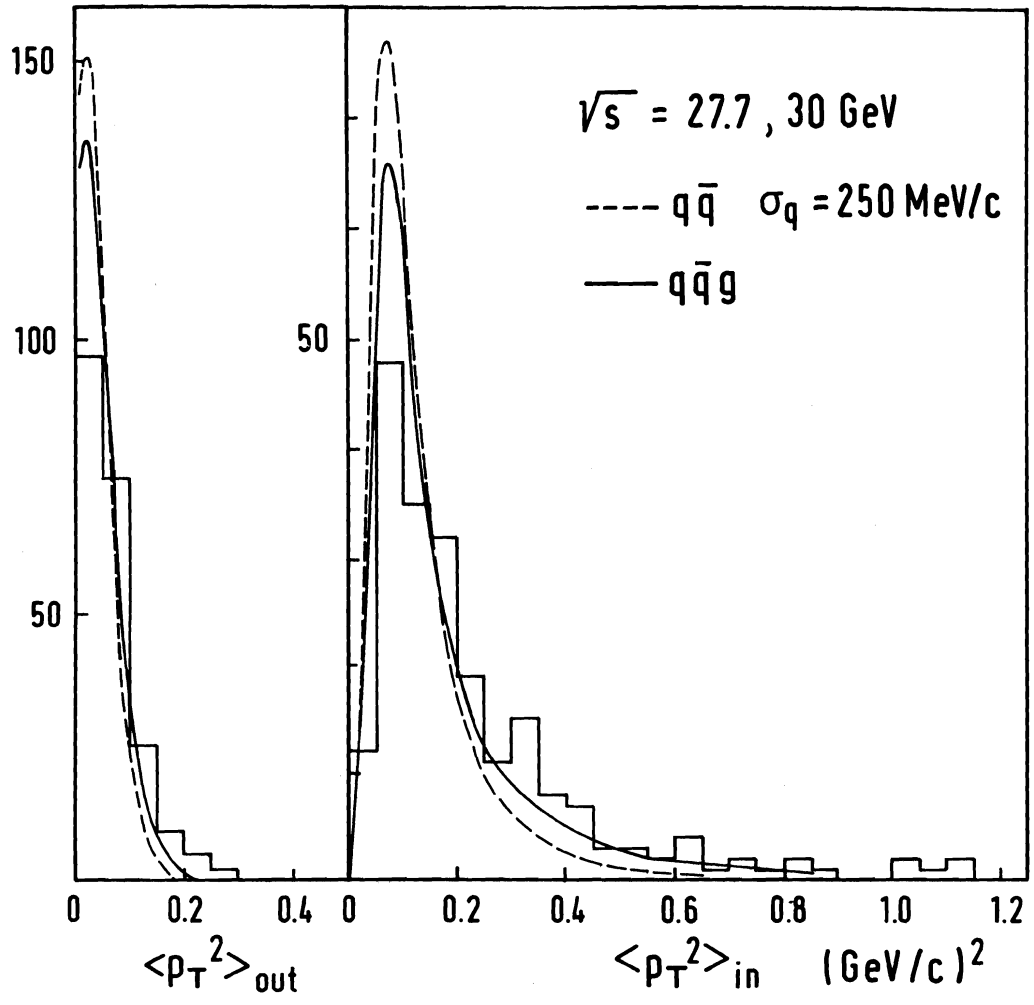

Fig. 11: Distributions of mean transverse momentum squared per event for charged particles, normal to ($\langle p_T^2 \rangle_{out}$) and in ($\langle p_T^2 \rangle_{in}$) the event plane.

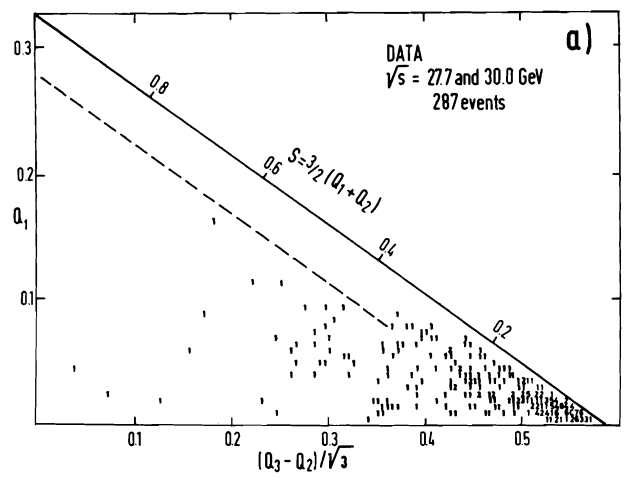

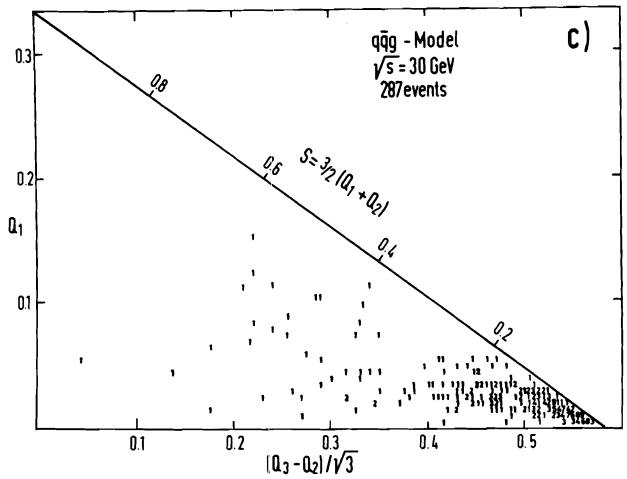

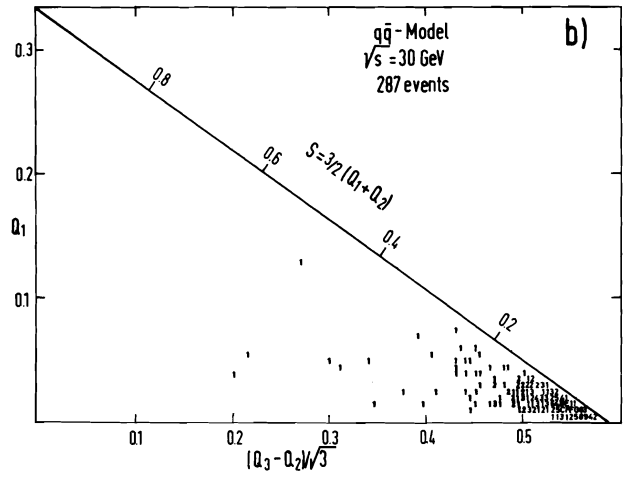

Fig. 12: "Event shape" Q-plot.

a) High energy data

b) $g\bar{g}$ model prediction with σ_g = 250 MeV/c

c) $g\bar{g}g$ model prediction

The planarity $(Q_2 - Q_1)$ axis is perpendicular to the sphericity axis. The dotted line indicates planarity = 0.07.

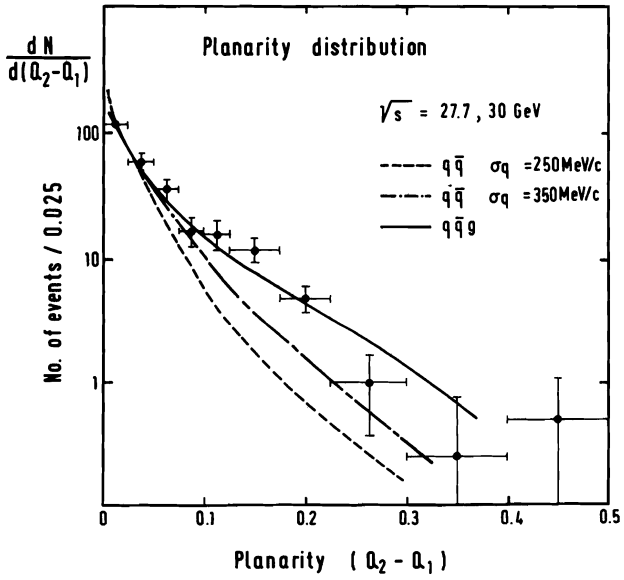

Fig. 13: The planarity distribution compared with model predictions.

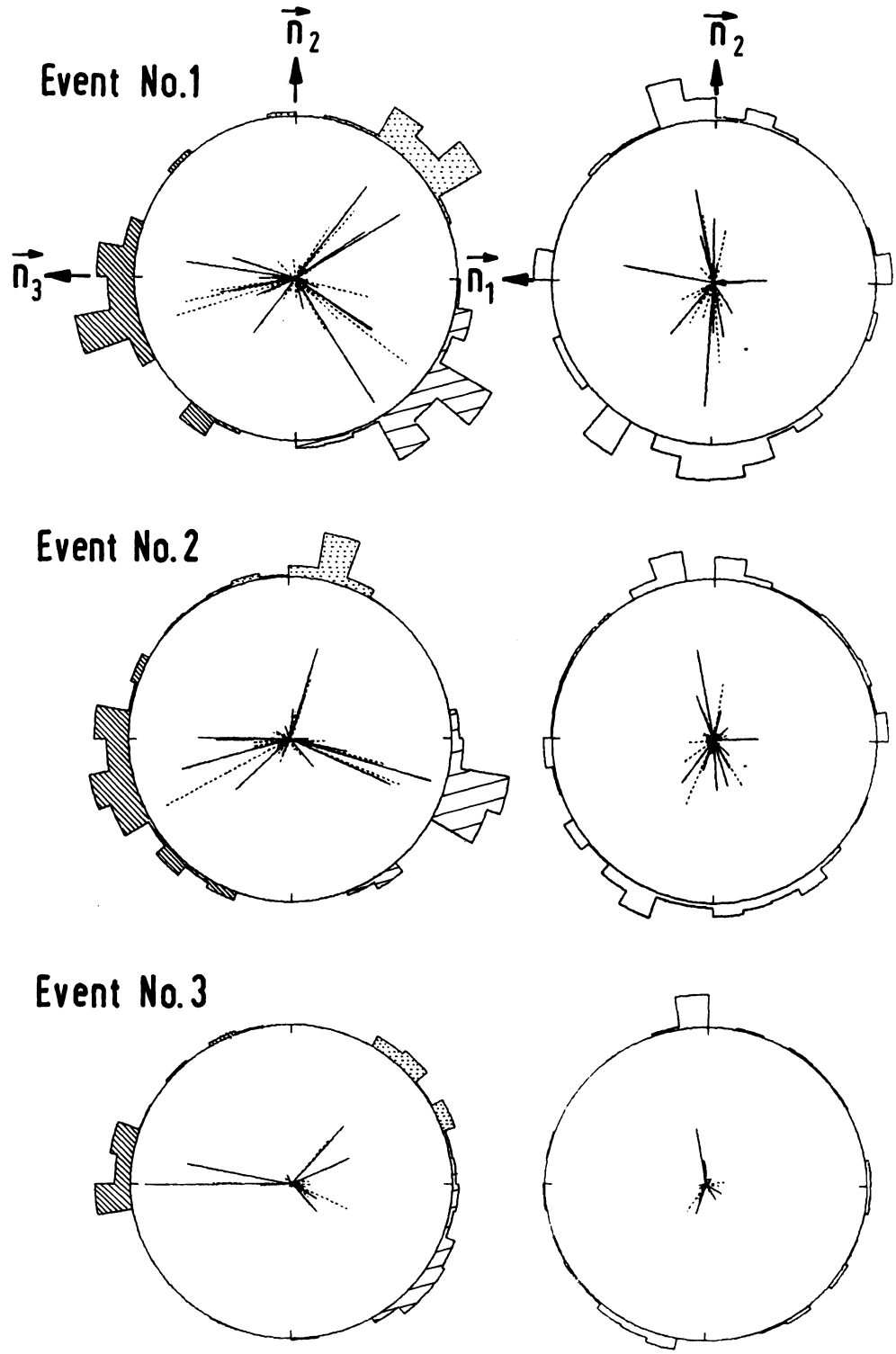

Fig. 14a): Typical three jet events projected onto the $(\vec{n}_3,\vec{n}_2)$ and $(\vec{n}_1-\vec{n}_2)$ planes. The full and dotted lines represent the momentum vectors of charged and neutral particles respectively. The energy flow is shown by the histograms plotted on a circle around each event. The three energy clusters obtained from a three-jet analysis are indicated in the $(\vec{n}_3,\vec{n}_2)$ projection of each event. Note that the momentum and energy scales are different for the three events.

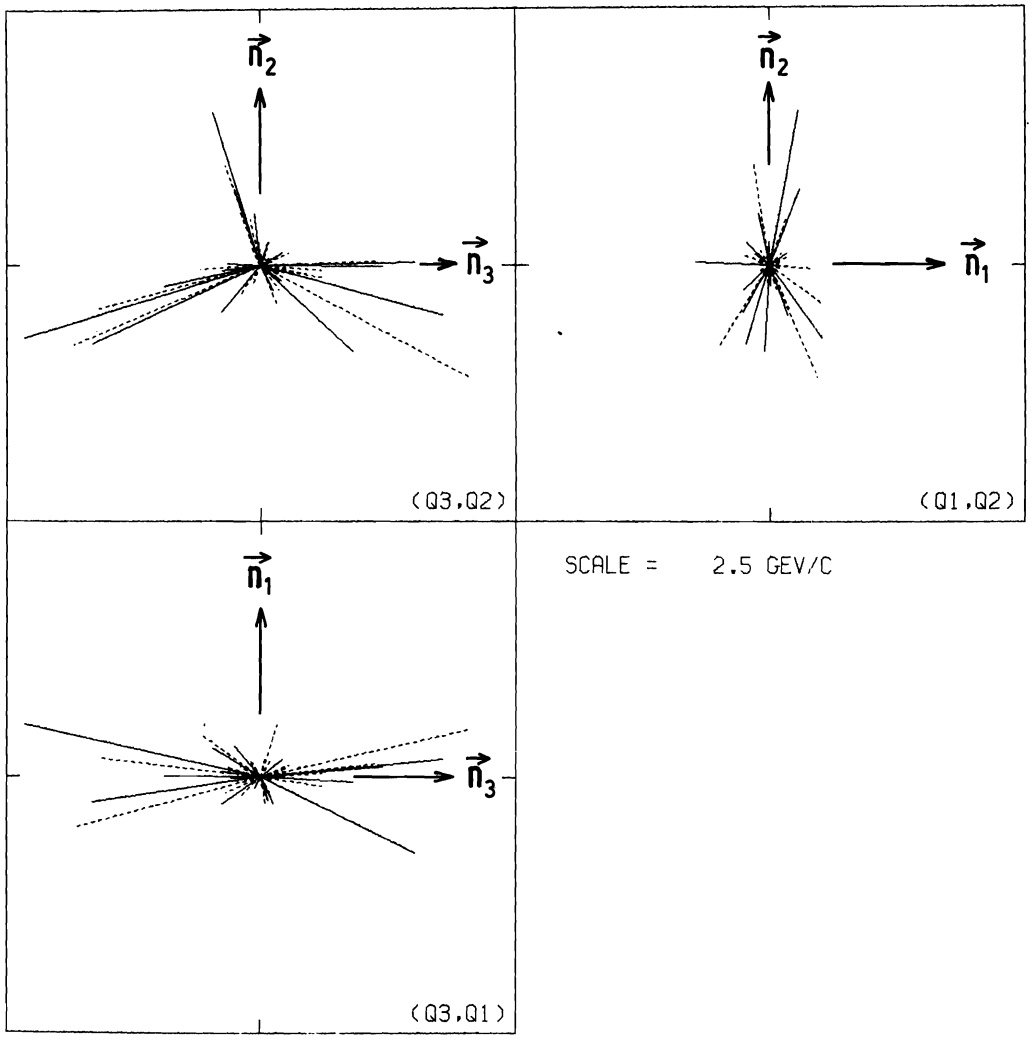

Fig. 14b): The three projections of event No. 2 from the previous figure onto the $(\vec{n}_3,\vec{n}_2)$ (top left), $(\vec{n}_1,\vec{n}_2)$ (top right) and $(\vec{n}_3,\vec{n}_1)$ (bottom) planes.

Table 4 Observed and expected numbers of planar events with $Q_2 - Q_1 > 0.07$

observed	expected		
	$q\bar{q}$ model σ_q = 250 MeV/c	σ_q = 350 MeV/c	$q\bar{q}g$ model
78 events	24 events	36 events	74 events

The detailed agreement observed in all of these figures and tables between data and $q\bar{q}g$ model predictions strongly suggests gluon bremsstrahlung as the origin of the planar three-jet events. The long tails observed in the thrust, $\langle p_\perp^2 \rangle_{in}$ and to the planarity distributions can be easily explained as hard components of the bremsstrahlung.

7. Search for Fractionally Charged or Heavy Stable Particles

The dE/dX information obtained by the Jet chamber provides the possibility of identifying particles even inside a jet. This feature of the JADE detector was applied in a search for fractionally charged or heavy stable particles whose ionization would be much different from that of the ordinary known particles. It should be noted that the previous searches[28] for such particles were mainly done in hadronic reactions, essentially at small q^2. This is a first search for such particles in e^+e^- annihilation at energies near $\sqrt{s}$ = 30 GeV.

The Jet chamber provides up to 48 ionization measurements along a track. To determine the dE/dX of a track we leave out the highest 20 % of the measurements and take the mean of the remaining 80 %. As shown in fig. 15a and b, this method of the truncated mean suppresses the effect of the Landau tail and provides a dE/dX resolution of ± 6 % , as measured for the $e^\pm$ particles from Bhabha scattering.

The dE/dX for each track obtained in this way are plotted in fig. 16 versus the observed momentum of the track. All tracks containing at least 30 points from all multihadron candidates have been entered into this figure[31]. No attempt was made to reject the small number of tracks produced by nuclear interactions in the material in front of the chamber. The curves[29] expected for ordinary particles (π, K, p) are plotted in fig. 16 together with curves for various fractionally charged particles and for heavy stable particles with a unit charge. The data show no accumulation of points outside the clearly visible bands of ordinary particles (π, K, p). Upper limits (90 % confidence level) on the production cross section for the hypothetical particles are summarized in table 5. As shown in this table the upper limits apply for a limited region of the momentum, excluding the range where the expected curves overlap with the bands of ordinary particles. For the particles with charge 1/3 the higher momentum range was also excluded in order to require a high dE/dX and, therefore, a high efficiency in the Jet chamber. The thresholds for the chamber electronics were set at 1/7 of the ionization from minimum ionizing particles emitted at a polar angle of 90° to the beam.

If bottom mesons (B) were produced in multihadronic events with a sufficiently long life time[30], they would be recognized as heavy stable particles with charge 1. No evidence is obtained for such particles, and an upper limit of 3×10^{-9}sec is deduced for the life time of the B meson assuming a mass of 5 GeV, a $B\bar{B}$ production cross section of $\Delta R = 1/9$ and a flat momentum distribution of B mesons predicted by the $q\bar{q}$ model.

Table 5 Upper limits ΔR on the inclusive production cross section (in units of the point-like μ pair production cross section) of fractionally charged or heavy stable particles

charge	mass GeV	range of the true momentum GeV/c	upper limit ΔR
1/3	3	1.5 < p < 2	0.1
	5	2 < p < 3	0.1
	10	1 < p < 7	0.1
2/3	3	p < 1 and p > 3.5	0.1
	5	p < 2 and p > 4	0.1
	10	p < 4.5 and p >10	0.1
1	3	p < 2	0.08
	5	p < 6	0.08
	10	p < 10	0.08

8. Angular Distribution of Jet Axes and indication for beam polarization

The angular distribution of inclusive hadrons and of jet axes was studied in a search for effects of possible beam polarization. Fig. 17 shows the azimuthal angular distributions of inclusive hadrons at $\sqrt{s}$ = 30 GeV. A $\cos 2\phi$ like modulation with its minima in the vertical directions is persistently observed, both for neutral and for charged hadrons and for various momentum and polar angle cuts. Each distribution in this figure can actually be fitted well with a function of the type $A + B \cos 2\phi$.

The same $\cos 2\phi$ modulation is also observed for the jet-axis distribution as seen in fig. 18. This figure shows the azimuthal angular distribution of the thrust axis for highly jet-like events (thrust > 0.85) inside the cut $|\cos\theta| < 0.5$.

Various checks[32] were performed to test whether this modulation could be explained by some defficiencies in the detector or in the analysis program. No such indication was observed.

The explanation for this azimuthal angular distribution of the jet axis can be a transverse polarization of the initial $e^\pm$ beams. The jet-axis distribution should then follow[16]

$$d\sigma/d\cos\theta\, d\phi \propto 1+\cos^2\theta + h_\perp^2 \sin^2\theta \cos 2(\phi-\Delta) \qquad (1)$$

where $h_\perp$ and Δ are respectively the transverse components of the beam polarization and a possible phase shift of the transverse component from the vertical direction. The above formula is based on the assumption that the highly jet-like events proceed via the process $e^+e^- \to q\bar{q}$ and subsequent quark fragmentation. Quarks are assumed to have spin 1/2 and negligibly small masses compared to $\sqrt{s}$. The jet axis is assumed to preserve the initial quark direction.

A maximum likelihood analysis was performed using the above formula for the data points $(\cos\theta_i, \phi_i)$, where θ_i, ϕ_i are the angles of the jet (thrust) axis for i-th events. A thrust cut T > 0.85 is applied to select only highly jet-like events. Events at small polar angles ($|\cos\theta| > 0.8$) were excluded in order to eliminate a possible edge effect of the detector. The maximum likelihood method resulted in $\Delta = -10 \pm 14°$ and $h_\perp^2 = 0.72 \pm 0.25$.

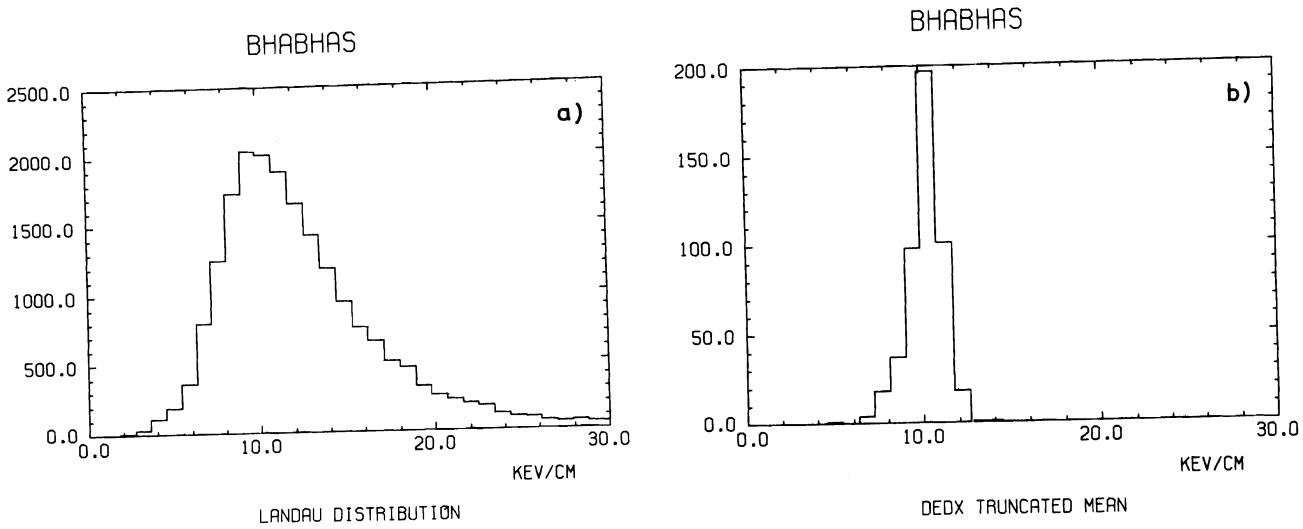

Fig. 15: dE/dx distributions for $e^{\pm}$ from Bhabha scattering:

a) dE/dx distribution (one entry per point)

b) Distribution of mean dE/dx for entire tracks. The lowest 80% of the dE/dx measurements along each track are the mean.

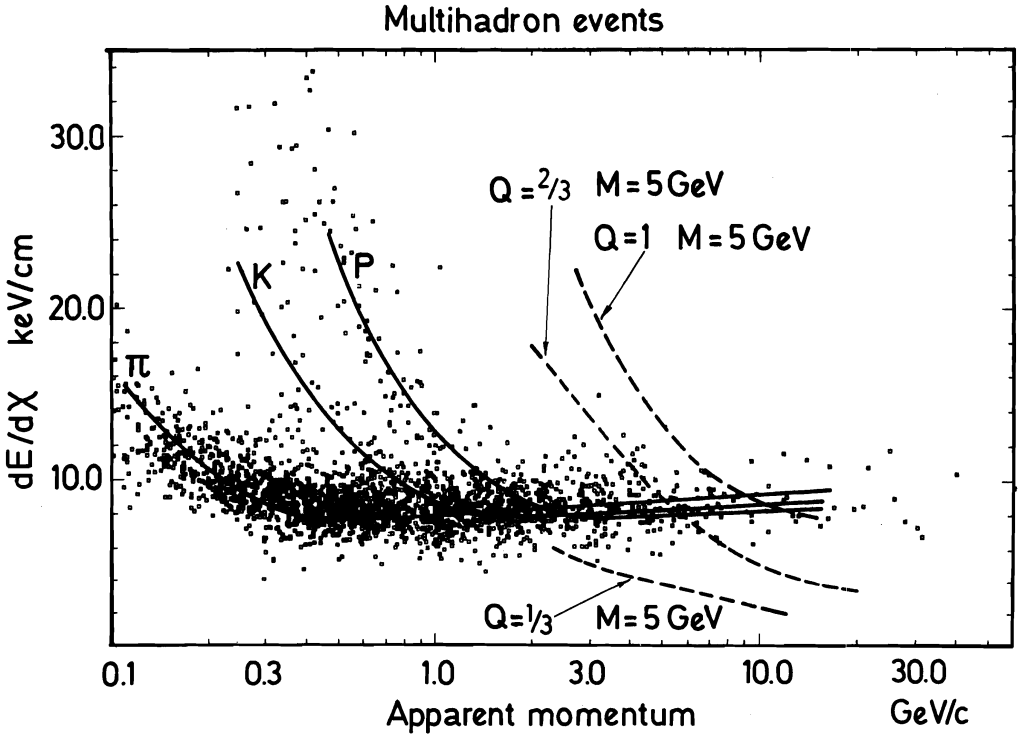

Fig. 16: dE/dx versus apparent momentum for all tracks in multihadron events with at least 30 hits.

The full and dotted lines represent respectively curves expected for ordinary (π,K,P) particles and for fractionally charged or heavy stable particles.

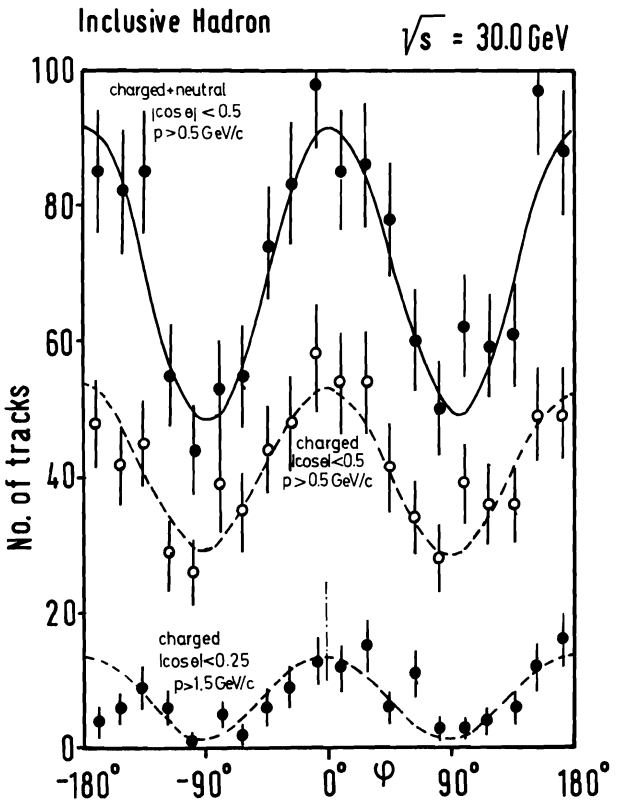

Fig. 17: Azimuthal angular distributions of inclusive charged and neutral hadrons at $\sqrt{s}$ = 30.0 GeV for various cosθ and momentum cuts. The curves represent fitted results using a formula of type A + B cos2φ.

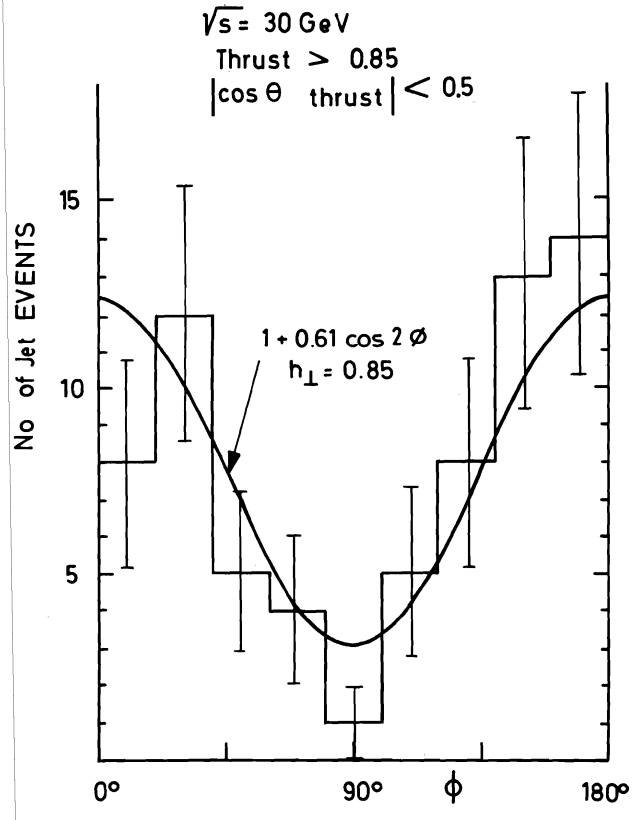

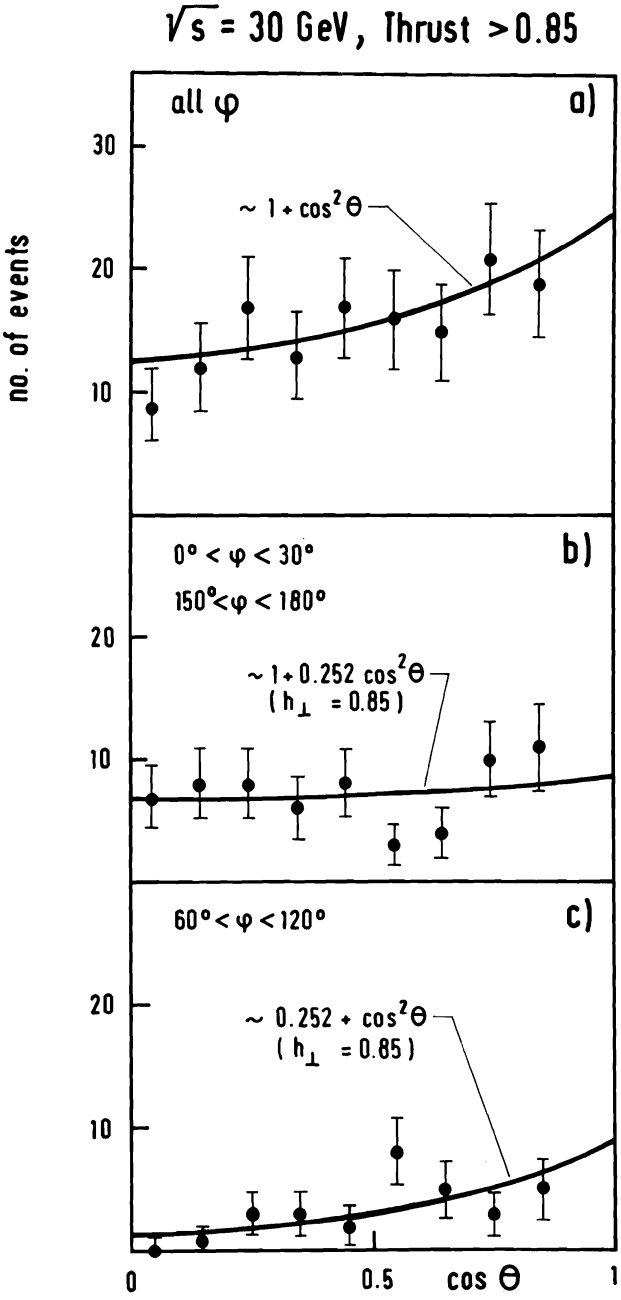

Fig. 19: Cosθ distribution of the jet axes; a) integrated over all φ, b) in the φ region near the horizontal direction, and c) near the vertical direction.

Fig. 18: Azimuthal angular distribution of jet (thrust) axes for jet like events. The curve represents the distribution expected for a transverse beam polarization of 0.85.

The following checks were performed to test the consistency of the data with the formula (1). The curve drawn in fig. 18 represents the ϕ-distribution of the jet axes obtained from an integration of the formula with a Δ value of 0 and a h_1 value of 0.85. The data agree well with the expected curve. Fig. 19 shows $\cos\theta$ distributions of the jet axes integrated over all ϕ (fig. 19a) and for two limited regions of ϕ near the horizontal (fig. 19b) and vertical (fig. 19c) directions. Also shown in the figure are the curves expected from proper integrations of (1) with the above mentioned Δ and h_1 values. Good agreements are observed between the expected curves and the data.

Therefore, at $\sqrt{s}$ = 30 GeV the jet axes show ϕ and $\cos\theta$ distributions consistent with a high transverse beam polarization. Detailed agreement between the data and the expected distributions support the assumed spin 1/2 nature of the quarks.

9. Conclusions

1) Validity of QED and the point-like nature of $e^{\pm}$ are tested to distances of 2×10^{-16} cm.

2) R values (total hadronic cross section in units of the point-like μ pair production cross section) are measured to be about 4 at $\sqrt{s}$ from 22 to 31.6 GeV. This value is compatible with the production of quarks with only the known flavours.

3) No evidence is obtained for events with spherical hadron distribution. Open top production is unlikely at $\sqrt{s}$ below 30 GeV.

4) Planar events are observed at a level far above the statistical fluctuations of the two-jet process. The planar events exhibit distinct three-jet structure in many cases. This proves that a fraction of the e^+e^- annihilations proceed via a three-body primary process and subsequent fragmentations of the three primary particles.

5) Quantitative as well as qualitative properties of the planar three-jet events agree in detail with the predictions based on the gluon bremsstrahlung process $e^+e^- \to q\bar{q}g$ and the subsequent fragmentations. This strongly suggests hard gluon bremsstrahlung as origin of the planar three-jet events.

6) No evidence is seen for fractionally charged or heavy stable particles produced in multihadron events.

7) The angular distribution of the jet axes indicates a transverse polarization of the beams at $\sqrt{s}$ = 30 GeV.

List of References

1. W. Bartel, T. Canzler, D. Cords, P. Dittmann, R. Eichler, R. Felst, E. Gadermann, D. Haidt, S. Kawabata, H. Krehbiel, B. Naroska, L.H. O'Neill, J. Olsson, P. Steffen, W.L. Yen
Deutsches Elektronen-Synchrotron DESY, Hamburg, Germany

E. Elsen, M. Helm, A. Petersen, H. Riege, P. Warming, G. Weber
II. Institut für Experimentalphysik der Universität Hamburg, Germany

H. Drumm, W. Farr, J. Heintze, G. Heinzelmann, R.D. Heuer, J. von Krogh, P. Lennert, H. Matsumura, T. Nosaki, H. Rieseberg, A. Wagner
Physikalisches Institut der Universität Heidelberg, Germany

J. Allison, J. Armitage, I. Duerdoth, F. Loebinger, A. Macbeth, H. Mills, D. Mercer, P.G. Murphy, H. Prosper, K. Stephens
University of Manchester, England

D.C. Darvill, F. Foster, G. Hughes, H. Wriedt
University of Lancaster, England

D. Clarke, M.C. Goddard, R. Hedgecock, R. Marshall, G.F. Pearce
Rutherford Laboratory, Chilton, England

M. Imori, T. Kobayashi, S. Komamiya, M. Koshiba, M. Minowa, S. Orito, A. Sato, T. Suda, H. Takeda, Y. Totsuka, Y. Watanabe, S. Yamada, C. Yanagisawa
Lab. of Int. Coll. on Elementary Particle Physics and Department of Physics, University of Tokyo, Japan

2. JADE collaboration, Proposal for a compact magnetic detector at PETRA, Sept. 1976.
The concepts and the basic design of the detector were already presented at the Discussion Meeting for PETRA Experiment by the Tokyo group (presented by S.Orito) and by the Heidelberg group (presented by J.Heintze); pages G43 and G60, Proceedings of the Discussion Meeting for PETRA Experiments, Frascati (March 1976)
3. W. Farr et al., Nucl. Instr. and Meth. 156 (1978) 283
H. Drumm et al., IEEE Trans. NS 26.1 (1979) 81
4. G. Bonneau and F. Martin, Nucl. Phys. B27 (1971) 381
5. K. Sauerberg, thesis, DESY F22-79/01 (unpublished)
6. F.A. Berends et al., Nucl. Phys. B61 (1973) 414
F.A. Berends et al., Nucl. Phys. B68 (1974) 541
F.A. Berends et al., Phys. Lett. 63B (1976) 432
7. A. Litke, Harvard University, Ph. D. Thesis (unpublished) (1970)
8. S.D. Drell, Ann. Phys. 4 (1958) 75
T.D. Lee and G.C. Wick, Nucl. Phys. B9 (1969) 209
9. S. Weinberg, Phys. Rev. Letters 19 (1967) 1264
A. Salam, Elementary Particle Physics, ed. N. Svartholm (Almkvist and Wicksell, Stockholm, 1968)
10. E.H. de Groote, G.J. Gounaris and D. Schildknecht, Bielefeld report, BI-TP 79/15
11. S.J. Brodsky, T. Kinoshita and H. Terazawa, Phys. Rev. D4 (1972) 1532
12. R.D. Field and R.R. Feynman, Nucl. Phys. B163 (1978) 1
13. T. Sjöstrand, B. Söderberg, Lund Report LU TP 78-18 (1978)
T. Sjöstrand, Lund Report LU TP 79-8 (1979)
14. T. Meyer, private communication
A. Ali et al., Zeit. f. Phys. C2 (1979) 33
15. P. Hoyer et al., DESY preprint DESY 79/21 (1979)
16. J. Ellis, Proc. of Summer Inst. on Particle Physics SLAC-215 (1978)
K. Koller et al., DESY Internal Report DESY T-79/01 (1979)
17. J.-E. Augustin et al., Phys. Rev. Lett. 34 (1975) 764
R. Brandelik et al., Phys. Lett. 76B (1978) 361
R. Brandelik et al., Phys. Lett. 83B (1979) 261
D.P. Barber et al., Phys. Lett. 83B (1979) 261
D.P. Barber et al., Phys. Rev. Lett. 43 (1979) 901
18. Barnett, Dine and McLerran, private communication
19. Except possibly for the data at $\sqrt{s}$ = 13 GeV from PLUTO, TASSO and MARK-J, which, if combined, show a 3σ deviation from the expected R value of about 4.
20. J.-E. Augustin et al., Phys. Rev. Lett. 34 (1975) 76
R. Brandelik et al., Nucl. Phys. B148 (1979) 189
C. Berger et al., Phys. Lett. 82B (1974) 449
21. E. Fermi, Prog. Theo. Phys. 5 (1950) 570 and Elementary Particles, New Haven, Yale University Press (1951) 86
22. J.D. Bjorken and S.J. Brodsky, Phys. Rev. D1 (1970) 1416
G. Hanson et al., Phys. Rev. Lett. 35 (1975) 1609
Ch. Berger et al., Phys. Lett. 82B (1979) 449
23. M. Kobayashi and K. Maskawa, Pro. Theor. Phys. 49 (1973) 652
24. J. Ellis et al., Nucl. Phys. B111 (1976) 253
T.A. De Grand et al., Phys. Rev. D16 (1977) 3251
25. G. Hanson et al., Phys. Rev. Lett. 35 (1975) 1609
G. Hanson, XIII Rencontrê de Moriond, Les Acres (1978), SLAC-PUB-s118 (1978)
Ch. Berger et al., Phys. Lett. 78B (1978) 176
Ch- Berger et al., Phys. Lett. 81B (1978) 410
D. Barber et al., Phys. Rev. Lett. 42 (1979) 1113
R. Brandelik et al., DESY 79/14 (1979)
26. S. Brandt et al., Phys. Lett. 12 (1964) 57
E. Fahri, Phys. Rev. Lett. 39 (1977) 1587
A. De Rujula et al., Nucl. Phys. B138 (1978) 387
27. For further analysis of the QCD effect the data at $\sqrt{s}$ = 27.7 GeV and 30 GeV were combined. The poor statistics data at the lowest (22 GeV) and the highest (31.6 GeV) energies were not included in view of the expected strong dependence of the effect on $\sqrt{s}$.
28. A comprehensive review of quark search experiments is given by: L.W. Jones, University of Michigan preprint DM HE 76-42 (1976)
29. W.W.M. Alison et al., N.I.M. 133 (1976) 321
30. D. Cutts et al., Phys. Rev. Lett. 41 (1978) 363

31. A dE/dX resolution (r.m.s.) of ±10 % is obtained from the width of the pion band compared to ±6 % obtained for $e^{\pm}$ from the Bhabha scattering. This broadening of the dE/dX resolution is mainly due to multi-tracks which hit a wire. The Jet chamber electronics are capable to measure up to eight ionizations from eight tracks using an 8 channel analogue memory per wire. These analogue memories were not thoroughly calibrated at the time of this analysis except for the first channels. Accurate calibration of these analogue memories is presently being carried out. This should improve the dE/dX resolution for multihadron tracks to a level similar to the resolution obtained for $e^{\pm}$ from the Bhabha scattering.

32. It is unlikely that the effect is due to local inefficiencies of detector components since a) both the charged and neutral particles exhibit the same modulation and b) $e^{\pm}$ from Bhabha scattering do not show a significant ϕ dependence within the statistical accuracy. To check the analysis program, Monte Carlo events with a flat ϕ distribution were generated and analysed in exactly the same way as the real data. This resulted in a flat ϕ distribution. Furthermore the jet events were visually scanned and the azimuthal angles of the jets were determined by eye. The resulting azimuthal angles exhibit the same $\cos 2\phi$ modulation.